16 Velocity, v1 and v2

16.1 Sensor

The airfoil probes are constructed in the manner developed by *Oakey* [1977] and shown in Fig. 34. One end of a bimorph beam is potted directly in hard epoxy, and the remainder

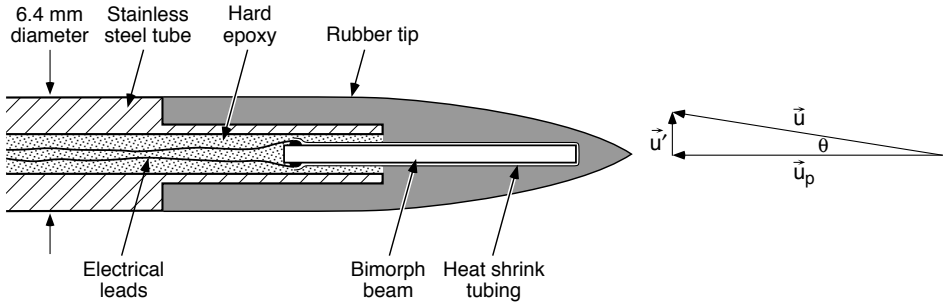

Figure 34: Schematic of airfoil probe used on MMP. For MMP, the probe velocity is the fall rate, w, and u' is any horizontal velocity relative to the MMP.

is encased in the soft rubber tip. The beams have high impedance, with resistances of about 10^{13} Ω, and capacitances of $C_S \approx 1000$ pF. Bending a beam in the direction of its sensitive axis produces a voltage. *Osborn and Crawford* [1980] describe the probes and their sensitivities. Each AMP carries two airfoils, both oriented with their sensitive axis in the same direction so their outputs can be compared during data editing; impacts of plankton on the probes are major causes of noise, and few impacts are simultaneous on both probes.

The rubber tips are made with parabolic cross-sections to provide constant lift for velocities u' parallel to the sensitive axis. The output voltage is

$$E_0(t) = S_v \left(\frac{V^2}{2g}\right) \frac{u'(t)}{V} \quad [V] \ , \tag{66}$$

where S_v is the probe sensitivity, and g is the gravitational constant. Typical sensitivities are $S_v = 18$ to 30 volts per meter.

The probes must be calibrated before and after cruises. This consists of measuring C_S with a precision capacitance meter and determining S_v using Oakey's procedure of placing them in a steady water jet having speed V. Slowly oscillating the probes creates a cross-velocity by changing the angle of attack, θ. Owing to the small angles, $u'(t)/V \approx \sin\theta(t)$. In practice, $\theta(t)$ and $E_0(t)$ are sinusoidal, and S_v is determined from their peak amplitudes. As shown below, the probe capacitance, C_S, also affects gain and must be measured. The nominal capacitance is 1000 pF. Probe sensitivities and capacitances measured before and after the cruise typically differ less than 15%.

Oakey [1977] estimates the dynamic response of the airfoil probes as

$$H^2_{\rm Oakey}(f,w) = \frac{1}{1+(\lambda_{\rm c} f/w)^2} \quad , \quad \phi_{\rm Oakey}(f,w) = \tag{67}$$

with $\lambda_c = 0.02$ m and $k_3 = f/w$, which is the vertical wavenumber in cycles per meter (cpm). Based on laboratory comparisons with a laser Doppler velocimeter, *Ninnis* [1984] gives the transfer function as

$$H^2_{\text{Ninnis}}(f, w) = A_0 + x\left(A_1 + x\left(A_2 + x(A_3 + xA_4)\right)\right) \ , \tag{68}$$

where $x \equiv f/(wK_0)$. It is meant to be used only to 100 cpm, corresponding to 60 Hz at a typical fall rate of 0.6 m s^{-1}. The parameters are given in Table 13, and both probe responses are shown in Figure 35. We use the Oakey version.

Parameter	Value
K_0	140.0
A_0	1.000
A_1	-0.165
A_2	-4.763
A_3	5.900

Table 13: Parameter values for Ninnis's representation of the airfoil transfer function.

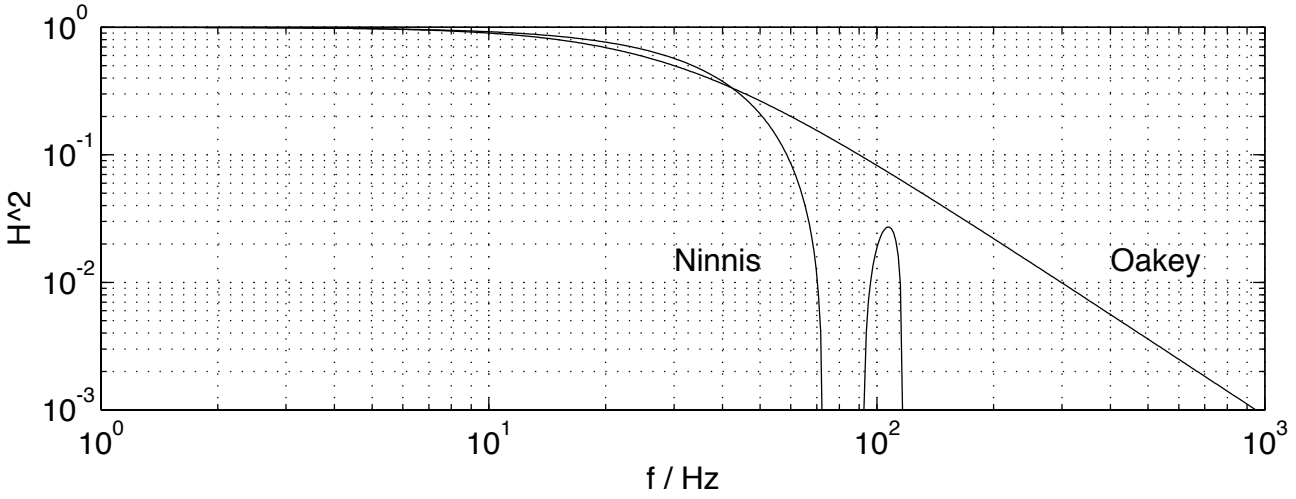

Figure 35: Transfer functions of the airfoil probe, with $w = 0.6$ m s^{-1}.

16.2 Electronics

The airfoil output voltage, E_0 is fed into three sequential circuits that buffer, differentiate, and amplify the signal (Figure 36). Circuit parameters are listed in Table 14.

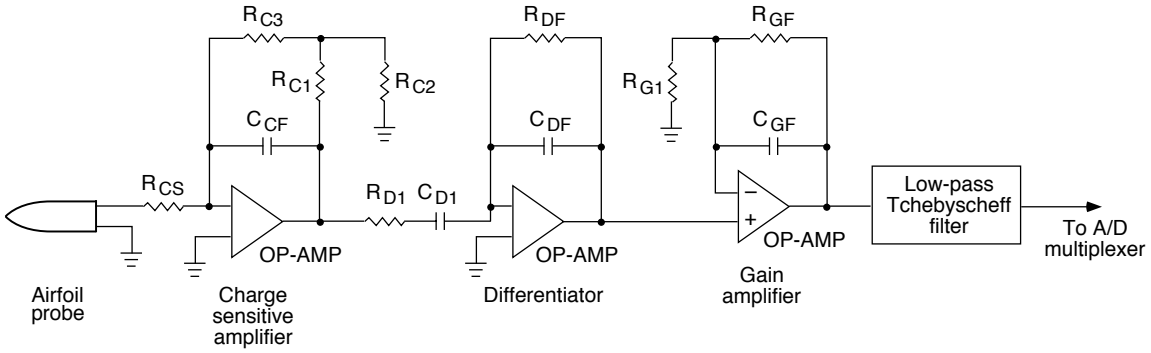

Figure 36: Schematic of airfoil circuits. The probe capacitance, C_S is between R_{CS} and common.

Component	Value	Component	Value
R_{C1}	$1 \times 10^6\ \Omega$	R_{DF}	$4.75 \times 10^5\ \Omega$
R_{C2}	$3.01 \times 10^3\ \Omega$	C_{DF}	8.2×10^{-10} F
R_{C3}	$1 \times 10^7\ \Omega$	R_{G1}	$1.21 \times 10^4\ \Omega$
C_{CF}	1×10^{-9} F	R_{GF}	$3.74 \times 10^4\ \Omega$
R_{D1}	$2.37 \times 10^3\ \Omega$	R_{CS}	$1 \times 10^5\ \Omega$
C_{D1}	3.3×10^{-7} F		

Table 14: Values of circuit components used with the airfoil probes.

The first stage is a charge-sensitive amplifier whose output matches its input voltage while supplying the current needed by the second stage. The power transfer function of the charge amplifier is

$$H^2_{\rm ca}(f, C_S) = \frac{(C_S/C_{CF})^2 (f/f_L)^2}{(1 + (f/f_L)^2)\,(1 + (f/f_H)^2)} \tag{69}$$

where

$$R_{\rm f} \equiv \frac{R_{C1} R_{C3}}{R_{C2}} = 3.32 \times 10^9\ \Omega \quad , \quad f_L \equiv (2\pi R_f C_{CF})^{-1} = 0.0479\ \text{Hz}\ , \tag{70}$$

and

$$f_H = (2\pi R_{CS} C_S)^{-1} \approx 1592\ [\text{Hz}]\ . \tag{71}$$

The response is unity at frequencies resolved by the airfoil probes and rolls off at lower and higher frequencies. The high-frequency rolloff is so much larger than frequencies of interest, that the term can be treated as a constant rather than being evaluated with C_S for each probe. We do not have an expression for phase as a function of frequency.

The second stage differentiates frequencies less than 100 Hz,

$$H^2_{\rm diff}(f) = \frac{K^2 f^2}{(f_1^2 + f^2)(f_2^2 + f^2)} \quad , \quad \phi_{\rm diff}(f) = \tan^{-1}\left(\frac{f_1 f_2 - f^2}{f(f_1 + f_2)}\right)\ , \tag{72}$$

where

$$K \equiv (2\pi R_{D1} C_{DF})^{-1} = 81,895 \text{ Hz} \ , \tag{73}$$

and

$$f_1 \equiv (2\pi R_{D1} C_{D1})^{-1} = 203.5 \text{ Hz} \quad , \quad f_2 \equiv (2\pi R_{DF} C_{DF})^{-1} = 408.6 \text{ Hz} \ . \tag{74}$$

It is plotted in Figure 37.

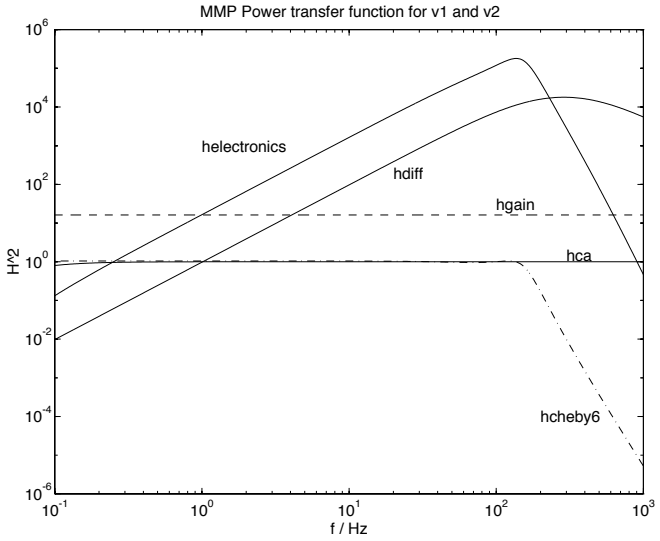

Figure 37: Power transfer functions for v1 and v2 electronics.

The third stage sets the gain with

$$H^2_{\text{gain}}(f) = \left(1 + \frac{R_{GF}}{R_{G1}}\right)^2 = 16.74 \quad , \quad \phi_{\text{gain}}(f) = 0 \ . \tag{75}$$

A 6-pole low-pass type 1 Tchebyscheff filter attentuates signals to minimize aliasing. The magnitude-squared response is given by (10).

The net electronic transfer function is the product of the seperate components

$$H^2_{\text{electronics}}(f, C_S) = H^2_{\text{ca}}(f, C_S)\, H^2_{\text{diff}}(f)\, H^2_{\text{gain}} \tag{76}$$

$$\phi_{\text{electronics}}(f) = \phi_{\text{hca}} + \phi_{\text{hdiff}} \tag{77}$$

It is plotted in Figure 37.

The total transfer function is

$$H^2_{\text{total}}(f, S_v, C_S, w, f_c) = \left(\frac{w S_v}{2g}\right)^2 H^2_{\text{electronics}}(f) H^2_{\text{Oakey}}(f, w) H^2_{\text{Tch}}(f, f_c) \quad [\text{volts}^2\ (\text{m/s})^{-2}] \ . \tag{78}$$

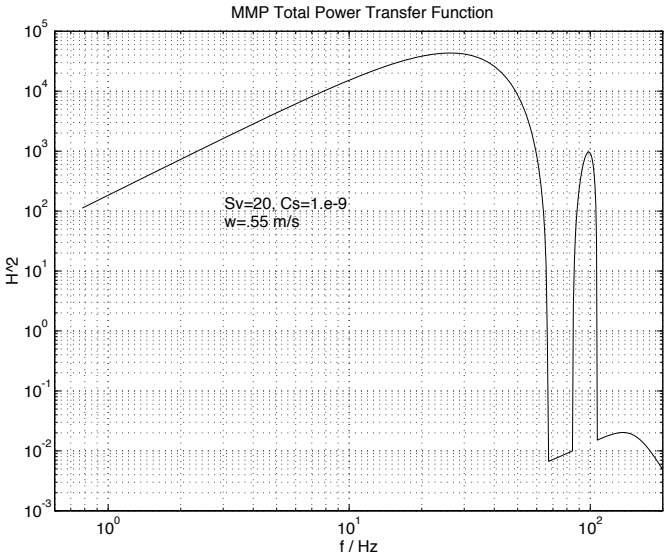

Figure 38: Total system power transfer function. Spectrum of raw v1 or v2 record in volts is divided by this to form a velocity spectrum in $\mathrm{m}^2\ \mathrm{s}^{-1}\ \mathrm{Hz}^{-1}$.

The scaling factor, $(wS_v/2g)^2$, comes from (66) and is about 0.58 for typical values of $S_v = 25$, $C_s = 1,000$ pF, and $w = 0.6$ m s^{-1}. It is shown in Figure 38.

Before 30 Jan 1995, the Tchebyscheff anti-alias filter had $f_c = 150$ Hz. On that day f_c was changed to 100 Hz. Spectra of raw data in volts^2 Hz^{-1} are divided by H^2_{total} to obtain velocity spectra in $\mathrm{m}^2\ \mathrm{s}^{-1}\ \mathrm{Hz}^{-1}$.

16.3 Data Conversion

16.3.1 Spectra

The power spectrum of recorded signals, converted to volts, is

$$\Phi_{\mathrm{R}}(f) = \frac{\Phi_u(k_3)}{w} H^2_{\mathrm{electronics}}(f, C_S) H^2_{\mathrm{Tch}}(f, f_c) H^2_{\mathrm{Oakey}}(f, w) \left(\frac{S_v w}{2g}\right)^2 \quad \left[\mathrm{V}^2\ \mathrm{Hz}^{-1}\right] . \tag{79}$$

Inverting gives the oceanic velocity spectrum,

$$\Phi_u(k_3) = \frac{w\Phi_{\mathrm{R}}(f)}{H^2_{\mathrm{electronics}}(f, C_S) H^2_{\mathrm{Tch}}(f, f_c) H^2_{\mathrm{Oakey}}(f, w)} \tag{80}$$

The spectrum of vertical shear is

$$\Phi_{\partial u/\partial z}(k_3) = (2\pi k_3)^2 \Phi_u(k_3) \quad \left[\mathrm{s}^{-2}\ \mathrm{cpm}^{-1}\right] . \tag{81}$$

The rate of viscous dissipation of turbulent kinetic energy, ϵ, is obtained by integrating the shear spectrum

$$\epsilon = 7.5\nu(s,T,P)\int_{k_0}^{k_u} \Phi_{\partial u/\partial z}(k_3)\,dk_3 \quad [\mathrm{W\,kg^{-1}}]\ , \tag{82}$$

where $\nu(s,T,P)$ is the kinematic viscosity, and k_0 and k_u are the lower and upper cutoffs determined by record length and the character of the data, respectively. Variations in ν are large enough that it should be evaluated at in-situ conditions.

The dissipation spectrum,

$$\phi_{\mathrm{diss}} = k_3\Phi_{\partial u/\partial z}(k_3) \quad [\mathrm{s^{-2}}]\ , \tag{83}$$

shows the relative contributions of different wavenumbers to ϵ if plotted with a logarithmic k_3 axis and a linear abscissa.

16.4 Observed Characteristics

BIBLIOGRAPHY

References

Bennett, R. S., The calibration of thermistors over the temperature range 0°C to 30°C, *Deep-Sea Res.*, *19*, 157–163, 1972.

Gregg, M., and T. Meagher, The dynamic response of glass rod thermistors, *J. Geophys. Res.*, *85*, 2779–2786, 1980.

Gregg, M., T. Meagher, A. Pederson, and E. Aagaard, Low noise temperature microstructure measurements with thermistors, *Deep-Sea Res.*, *25*, 843–856, 1978.

Irish, J. D., and M. D. Levine, Digitizing error from period and frequency counting techniques, *Deep-Sea Res.*, *25*, 211–219, 1978.

Ninnis, R., *The effects of spatial averaging on air-foil probe measurements of oceanic velocity microstructure*, Ph.D. thesis, Univ. of British Columbia, Vancouver, Canada, 1984.

Oakey, N. S., An instrument to measure oceanic turbulence and microstructure, Rept. Series BI-R-77-3, Bedford Inst. Oceanogr., Dartmouth, N.S., Canada, 1977.

Osborn, T. R., and W. R. Crawford, An airfoil probe for measuring turbulent velocity fluctuations in water, in *Air-Sea Interactions: Instruments and Methods*, edited by F. Dobson, L. Hasse, and R. Davis, 369–386, Plenum, New York, 1980.

Otnes, R. K., and L. Enochson, *Applied Time Series Analysis, Vol. 1: Basic Techniques*, Wiley, New York, N. Y., 1978.

Pederson, A., and M. Gregg, Development of a small *in-situ* conductivity instrument, *IEEE J. Ocean Engr.*, *OE-4*, 69–75, 1979.

Williams, A. B., *Electronic Filter Design Handbook*, McGraw-Hill, New York, 1981.